J. Fluid Mech. (1980), *vol.* 98, *part* 4, *pp.* 755–768
Printed in Great Britain

Double-diffusive instability in an inclined fluid layer. Part 1. Experimental investigation

By R. C. PALIWAL† AND C. F. CHEN

Department of Mechanical, Industrial and Aerospace Engineering,
Rutgers University, New Brunswick, N.J. 08903

(Received 21 May 1979 and in revised form 18 October 1979)

The stability boundary of a density-stratified fluid contained in an inclined slot subjected to a lateral temperature gradient was determined experimentally. The initial stratification due to salt was stable and linear in the vertical direction. Experiments were conducted in a $1{\cdot}0 \times 11{\cdot}1 \times 25{\cdot}7$ cm slot with the inclination angle θ from the vertical varying from $-75°$ to $+75°$. A positive angle denotes heating from the lower wall while a negative angle denotes heating from the upper wall. The temperature difference across the slot was increased slowly until the onset of instability was observed by means of a shadowgraph. The critical thermal Rayleigh number was found to be non-symmetrical with respect to $\theta = 0°$, with heating of the upper wall less stable than heating of the lower wall. This is because there is a larger vertical solute gradient in the steady-state regime prior to the onset of instabilities when the lower wall is heated. The secondary flow consisting of horizontal convecting layers was very stable in $\theta < 0°$ cases because of the stabilizing temperature effect. The motion of the layers when $\theta > 0°$ was quite vigorous. At $\theta = +75°$, the secondary flow became unstable in a rather dramatic manner not observed heretofore.

1. Introduction

When a stably stratified fluid layer is subjected to heating from below, the onset of instabilities is in the oscillatory mode. This phenomenon was predicted by Veronis (1965) and confirmed experimentally by Shirtcliffe (1969), and more recently by Wright & Loehrke (1976) using a cleverly devised boundary condition which closely approximated the theoretical one. The basic state prior to the onset of instabilities is quiescent. When a stably stratified fluid layer is subjected to a lateral temperature gradient, imposed by maintaining a temperature difference across two vertical plane walls, instability in the form of horizontal convecting layers results. This phenomenon was first observed by Thorpe, Hutt & Soulsby (1969) who also made an asymptotic stability analysis. Later Hart (1971) considered the stability problem satisfying the correct boundary conditions and found that, at high values of the solute Rayleigh number, his results became indistinguishable from those of Thorpe *et al.* In this case, the basic state prior to the onset of instabilities is no longer quiescent. It consists of a thermally driven flow up the hot wall and down the cold wall such that the horizontal density gradient is nearly zero. In contrast to the case of heating from below, the onset of instability is of the stationary type.

† Present address: Electronic Associates, Inc., West Long Branch, N.J. 07764.

0022–1120/80/4465–1150 $02.00

When a stably stratified fluid is confined within two parallel plane walls inclined with respect to the vertical and subjected to a temperature differential, several interesting factors come into play on the onset of instabilities. First, even without heating there are buoyancy layers along the two walls transporting fluid up and down (Phillips 1970). The thermally driven flows may augment or diminish the buoyancy-layer flow depending on whether the lower or the upper wall is being heated respectively. Secondly, depending on the position of the hot wall, the fluid may be subjected to a heating-from-below or heating-from-above effect which may influence the stability of the layer with respect to double-diffusive mechanisms.

Some of the effects of the combined flow due to density stratification and heating along a sloping wall have been investigated by Chen, Paliwal & Wong (1976). These experiments were performed with a stably stratified fluid in a large tank with one sloping wall. The basic state is a time-dependent one generated by impulsive heating of the sloping wall. The flow is always up the wall, peaking very close to the wall and decreasing rapidly away from the wall. The critical thermal Rayleigh number for this type of flow, based on reduced gravity ($g\cos\theta$) and natural length scale h (height of rise of a heated fluid parcel in the stratified surroundings; Chen, Briggs & Wirtz 1971), remains unchanged up to $\theta \simeq 60°$, and then it increases rapidly as θ further increases. At $\theta = 75°$, it is about three times the value at $\theta = 60°$. Stability calculations made by Chen (1978) confirmed the rather sharp increase in the critical thermal Rayleigh number as θ is increased beyond 60°.

Double-diffusive phenomena in a two-solute fluid in the presence of sloping boundaries have been investigated by Turner & Chen (1974), Chen (1975), Chen & Sandford (1977) and Linden & Weber (1977). Since the container walls are impervious to solutes, the basic state is necessarily time dependent. Because of the opposite gradients of two solutes with different diffusivities, the transient state may involve reverse flows which induce horizontal gradients of the solute in such a manner that double-diffusive instability results. The secondary flow consists of the ubiquitous horizontal convecting layers.

Recently, we have completed an experimental and theoretical study of double-diffusive instability in an inclined fluid layer. Experiments were conducted in a narrow tank which was inclined from the vertical at 0°, $\pm 30°$, $\pm 45°$, $\pm 60°$, and $\pm 75°$. Positive angles denote heating of the lower wall, while negative angles denote heating of the upper wall. A constant vertical salt stratification was maintained for all tests. Heating was gradual and sufficient time was allowed between increases of temperature difference across the slot so that a steady basic state is achieved prior to the onset of instabilities. In this paper our experimental work is presented. Readers who are interested in experimental details omitted here are advised to consult Paliwal (1979). Our theoretical work is presented in a companion paper (Paliwal & Chen 1980).

2. Experimental apparatus

The main part of the apparatus is the experimental tank (measuring $25{\cdot}7 \times 11{\cdot}1 \times 1{\cdot}0$ cm) shown in figure 1. The side walls ($25{\cdot}7 \times 11{\cdot}1$ cm) of the tank are 0·635 cm brass plates. The front and rear walls as well as the bottom are made of 0·635 cm Plexiglas. The brass plates are enclosed externally in water jackets which are 3·175 cm thick

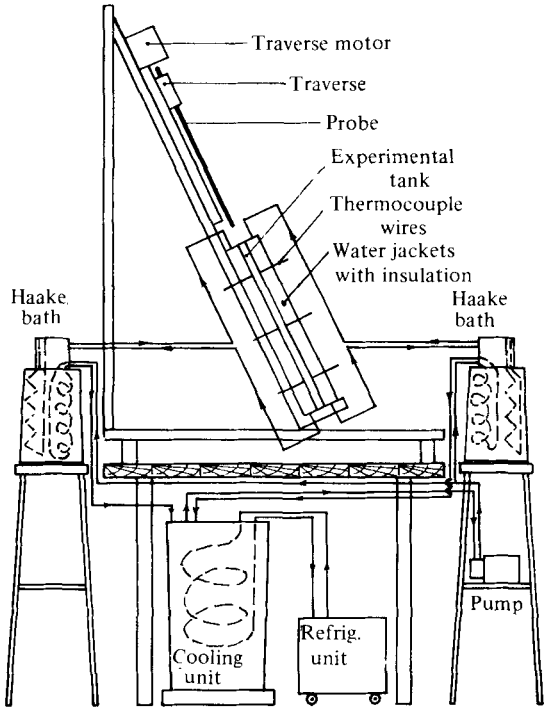

FIGURE 1. Sketch of experimental apparatus.

Plexiglas plates with water passages milled in them. In each water jacket, the circulating water enters at the top near the front as well as the rear of the slot, flows downward in two independent circuits, reverses its direction twice and leaves at the bottom near the middle of the brass plates (figure 2). This arrangement allows the entering water to flow first near the edges, where the heat losses or gains are expected to be maximum, thus ensuring better uniformity of temperature in the plates. Figure 2 also shows the location of 15 copper–constantan thermocouple measuring junctions embedded in each of the metal plates to a depth of about half the plate thickness measured from the outside. Good thermal contact is ensured by using epoxy paste mixed with aluminium powder as adhesive to affix the thermocouple beads into the plates. The Plexiglas water jackets are insulated from outside to minimize heat loss.

It is possible to maintain each of the heat transfer plates at any desired constant temperature through the respective water jackets. Haake constant-temperature baths are used to control the temperature of circulating water. Each Haake bath has a small electric heater as a source of heat, and circulating cold brine in a separate coil as a sink. The brine is cooled by an external cooling unit.

The experimental tank and the water-jacket assembly are mounted on a metal frame, with the provision that the entire assembly can be tilted to any desired inclination. Above the tank and in line with its central axis, there is a motorized traverse mechanism. This is used to traverse a probe along the length of the tank for the purpose of withdrawing fluid samples which are used to determine the density distribution inside the tank. The probe is a hollow and thin metal tube (about 0·1 cm outside

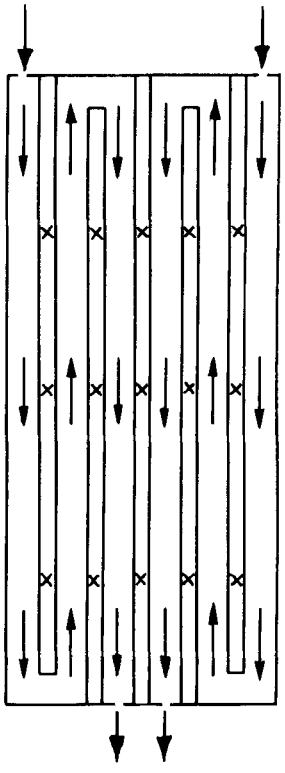

FIGURE 2. Path of circulating water and location of thermocouple junctions (×) on the constant-temperature metal plates.

diameter) inside a rigid glass tube (0·3 cm outside diameter). The lower 1 cm length of the metal probe is bent horizontally in order to withdraw the fluid sample from any desired horizontal level. The sample is withdrawn by means of a syringe connected at the other end of the probe using a small length of flexible tubing.

An apparatus, similar to the one used by Turner & Chen (1974) but involving two small Plexiglas cylindrical containers (15·24 cm high and 5·08 cm inside diameter) in place of the two buckets, was used for establishing the linear density gradient of salt in the experimental tank.

Other apparatus used consisted of a Hewlett–Packard digital multimeter (Model 3490A), a refractometer (American Optical, Model 10402 Concentricimeter), and a Nikon camera fitted with a microlens. The multimeter was used in conjunction with two selector switches to obtain temperatures at different locations on the brass plates of the experimental slot. An ice–water mixture in a thermos bottle was used as a reference junction for all the thermocouples. This eliminated errors due to uncertainty in the reference temperature, as far as relative magnitudes of temperature at different locations were concerned. The refractometer was used to determine the refractive indices of the fluid samples drawn for the purpose of checking the density distribution in the slot. Refractive indices of salt solutions of different densities are tabulated in the *Handbook of Chemistry and Physics* (Weast 1977–1978). The camera was used to record the onset and evolution of instability as seen on shadowgraphs at different times.

3. Procedure

3.1. *Establishing the initial salt gradient*

The initial vertical density gradient due to salt ϕ_0 ($= \beta|dS/d\zeta|_0$) was kept at a constant value, approximately 0·0052 cm^{-1}, for all tests. (The co-ordinate ζ is in the vertical direction and z is along the wall of the test tank.) This gradient corresponds to a variation of salt concentration between 0 % at the top and 20 % at the bottom of a vertical layer 25 cm in height. We used such a steep gradient so that the relatively large critical temperature difference across the slot could be measured with greater accuracy. Further, the salt concentration at mid-height was kept at 10 % for all tests. Thus, salt concentrations at the top and the bottom of the gradient region were different at different angles.

A layer of saturated salt solution was introduced at the bottom of the tank prior to the filling of the gradient region, and a layer of fresh water was introduced on top of the gradient region. Both layers were approximately 3 cm along the tank. Thus the gradient region was approximately 18 cm along the tank. The purpose of the saturated fluid layer at the bottom and the fresh water layer at the top was to avoid the possibility of early establishment of convecting cells near the top and bottom boundaries. In the absence of these homogeneous layers, regions near the top and bottom boundaries would tend to contain a smaller salinity gradient to satisfy the condition of zero flux at these boundaries. During the process of slow heating, these regions would therefore become unstable at a considerably lower temperature gradient than that required for the main stratified region. In fact, besides the lateral heating effect, experimental conditions near the hot vertical boundary were such that the bottom region was subjected to some heating from below and the top region was subjected to some cooling from above. Altogether, this would mean vigorously convecting and hence rapidly growing cells near the horizontal boundaries (Chen *et al.* 1971) during the process of slow heating. Such a situation would make the determination of the critical instability of the main stratified region extremely difficult. On the other hand, the presence of homogeneous layers introduced step changes in salinity at the upper and lower boundaries of the gradient region. Diffusion in the vertical direction at these boundaries made the upper and lower part of the gradient region much more stable than its middle part, where the initial value of the vertical density gradient remained unchanged for a sufficiently long time (Chen & Sandford 1976). Onset of instability, therefore, took place away from the upper and lower boundaries, in the middle region of known initial solute stratification.

Before introducing the temperature gradient in the fluid, the actual initial density stratification due to salt was determined to ensure its linearity. This was done by withdrawing small fluid samples every 2 cm along the length of the slot with the help of the sampling probe and the traverse mechanism. The refractive index of each sample was determined immediately by the refractometer, and later converted to density data. The distribution of density along the length of the slot for a typical run ($\theta = 45°$) is shown in figure 3. It can be seen that the linear gradient was achieved for about 12 cm of slot length, from 7 to 19 cm measured from the bottom of the slot. There are two very stable layers bordering on the linear gradient region. For each run, a least-squares straight-line fit was calculated for density data points in the estimated linear gradient region. The calculated slope divided by $\cos\theta$ was taken as the actual initial

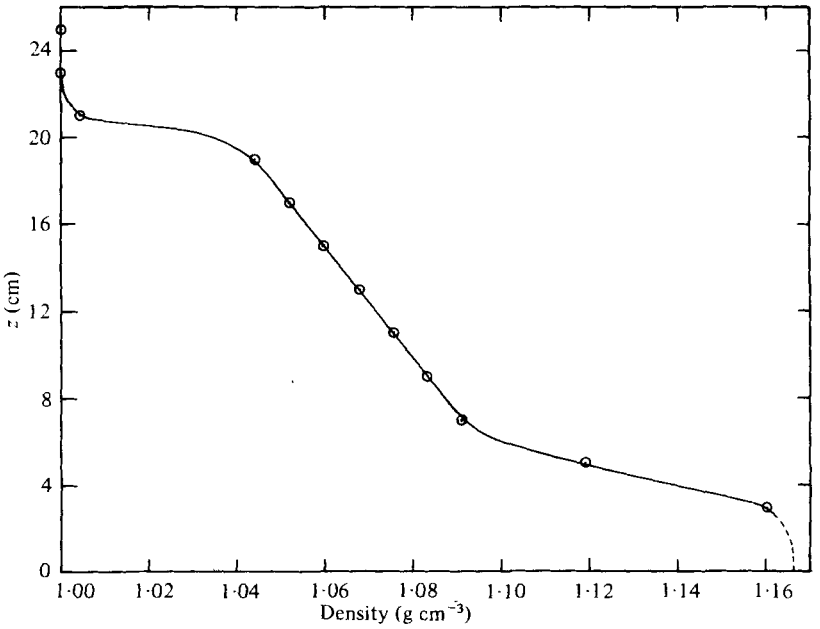

FIGURE 3. Initial density distribution in the experimental tank ($\theta = 45°$).

value of the vertical density gradient due to salt. Uncertainty in the density gradient, which is less than 8 %, may be caused by discrepancies in the filling process, as well as the method of determination of the density gradient.

3.2. *Differential heating*

Except for $\theta = 0°$ (vertical boundaries) experiments were made with the lower boundary heated (positive θ) as well as the upper boundary heated (negative θ). In the case of $\theta = 0°$, the left-hand boundary was heated. Initially, both boundaries as well as the fluid were at a uniform temperature close to room temperature. The temperature of one of the boundaries was then increased slowly in steps of approximately 0·5 °C every 5 min initially and later in smaller steps of 0·20–0·25 °C every 15 min near the state of critical instability (within about 0·5–1·5 °C). A rough estimate of the critical temperature was possible either with experience or on the basis of some trial runs made with larger temperature steps. Generally, it took about 3–4 min after changing the setting of the Haake bath to effect the desired temperature step at the heated boundary. The thermal diffusion time through the 1 cm width of the slot is about 11 min. The 15 min intervals in the final steps of temperature rise were thus sufficient to ensure steady state at each step. Earlier steps of 0·5 °C every 5 min were at considerably subcritical values of temperature difference. This relatively faster rate of heating in the beginning had no effect on the final outcome of the experiment when compared to several preliminary test runs in which each temperature increase was accompanied by a waiting period of 15 min.

It was important that during the heating process no significant temperature gradients existed within any of the metal heat transfer boundaries. The temperature at each of the 15 thermocouple locations in each of the plates was monitored continuously.

Maximum temperature difference between any two locations on the same plate was less than 0·1 °C.

During the final stages of the slow differential heating, the motion of the fluid in the slot was very carefully watched. The shadowgraph technique was used for flow visualization. This was done by covering the front Plexiglas with tracing paper and allowing uncollimated light from a 500 W slide projector to pass through the transparent walls of the tank. When inhomogeneities in the refractive index resulting from the motion of the fluid due to buoyancy effects became substantial, their advection may be visualized by the shadow on the tracing paper.

Onset of instability was evidenced by the sudden appearance of relatively bright and approximately horizontal lines on the shadowgraph. The bright lines below each interface indicate sharp changes in the refractive index of the fluid due to step-changes in the solute concentration of the fluid between the cells. These lines slowly sharpened, and were sometimes followed by the appearance of vortices, slightly closer to the hot wall than to the cold wall, in about 3–5 min from the onset of instability. The vortices soon transformed into very turbulent motion within the horizontal layers, which grew continuously in a cellular pattern. As soon as the onset of instability was first detected, no further rise in temperature difference was allowed and the growth of instability took place at a fixed value of temperature difference across the walls.

The critical temperature difference ΔT_c was taken as the mean of ΔT at the time of the first detection of instability and its value before the last step in temperature rise. These two ΔT values corresponded respectively to slightly supercritical and subcritical conditions of instability, and their average was considered closest to the true value of ΔT_c. The subsequent evolution of instability was recorded by still photography of the shadowgraphs at frequent intervals for about 1 h, and occasionally for a longer time with relatively larger intervals.

3.3. *Variation of fluid properties along the slot*

The thermal and solute Rayleigh numbers are defined as

$$R_T = \frac{g\alpha\Delta T D^3}{\kappa_T \nu}, \quad R_S = \frac{g\beta|dS/d\zeta|_0 D^4}{\kappa_T \nu},$$

in which g is the gravitational acceleration, α and β are volumetric expansion coefficients for heat and salt respectively, κ_T is the thermal diffusivity, ν is the kinematic viscosity, $|dS/d\zeta|_0$ is the initial vertical solute gradient, ΔT is the temperature difference across the parallel boundaries D apart. Since fluid properties are functions of salinity and temperature, R_T and R_S will vary across and along the slot. However, within the temperature range used, variations of R_T and R_S due to temperature are quite small. Figure 4 shows values of R_T and R_S, near the critical state for $\theta = 0°$, that may exist at different locations in the slot along its length. Besides the experimental variation of R_T due to variations in fluid properties, predicted values of $R_{T,c}$ according to the asymptotic formula of Thorpe *et al.* (1969)† are also shown. For the case illustrated, the salt density gradient $\phi_0 = 0{\cdot}0052\ \mathrm{cm}^{-1}$, and temperature difference $\Delta T = 5{\cdot}0\ °\mathrm{C}$, which correspond approximately to the critical conditions for $\theta = 0°$.

† It is noted that Rayleigh numbers are defined somewhat differently in this paper.

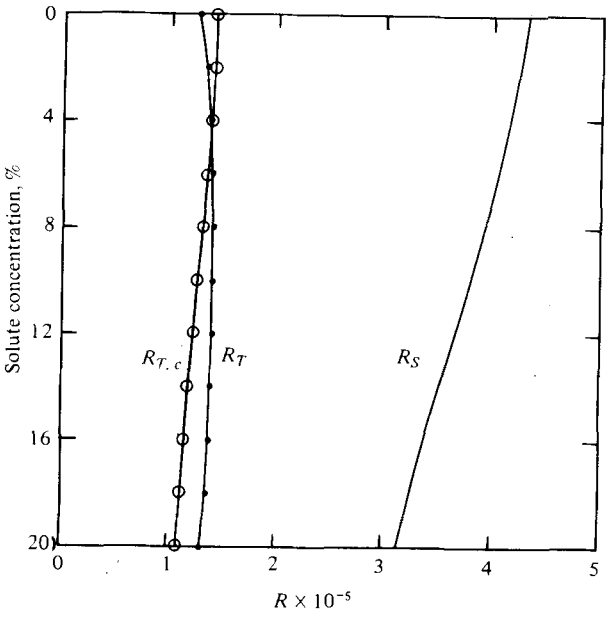

FIGURE 4. Variation of R_T and R_S with solute concentration in the test tank. The initial density gradient $\phi_0 = 0{\cdot}0052$ cm^{-1} and the temperature difference $\Delta T = 5{\cdot}0$ °C. The critical thermal Rayleigh number $R_{T,c}$ is calculated according to the asymptotic analysis of Thorpe *et al.* (1969).

However, for simplicity, no account of the top and bottom homogeneous layers has been taken.

It is observed that, for a given ΔT, R_T is maximum in the middle of the slot height, while R_S is maximum at the top and decreases monotonically toward the bottom. The critical thermal Rayleigh number, $R_{T\,c}$, as predicted by the asymptotic theory is a function of R_S. It too decreases from top to bottom at a rate comparable to that of R_S. As the temperature difference ΔT is slowly increased from subcritical to supercritical value, instability should first appear in the bottom half of the slot where more favourable conditions for critical instability exist. Once the instability sets in, it should progress slowly upward even without further rise in ΔT.

In most of the experimental runs, the onset of instability did start below the mid-height of the slot and progressed upward. If the step-change in the temperature difference near the critical state happened to be so big that the conditions in the entire slot became suddenly supercritical, the occurrence of instability was simultaneous throughout the slot. Experiments of Thorpe *et al.* (1969) with steady-state heating and those of Chen *et al.* (1971) and Chen & Skok (1974) with impulsive heating also show the appearance of layers starting close to the bottom of the tank, especially in runs near the marginal state.

4. Results and discussion

A total of 21 experiments were carried out, at least 2 for each inclination angle ($\theta = 0°$, $\pm 30°$, $\pm 45°$, $\pm 60°$, $\pm 75°$). The test conditions and fluid properties, the critical thermal Rayleigh number, the critical wavelength in the vertical direction, $\lambda_v = \lambda \cos\theta$, and the natural length scale h (Chen *et al.* 1971) are listed in table 1. The

Run no.	Angle ($\theta°$)	Average T (°C)	ΔT (°C)	$\phi_0 \times 10^2$ (cm^{-1})	$\alpha \times 10^3$ (°C^{-1})	$\nu \times 10^2$ (cm^2 s^{-1})	$\kappa_T \times 10^2$ (cm^2 s^{-1})	$R_S \times 10^{-3}$	$R_T \times 10^{-3}$ (critical)	h (cm)	λ_v (cm)	λ_v/h
29	−75	28·7	6·84	0·514	0·383	0·932	0·150	359	183	0·510	0·32	0·63
30	−75	28·6	6·85	0·538	0·383	0·933	0·150	376	183	0·488	0·36	0·74
27	−60	27·7	5·69	0·502	0·379	0·951	0·150	345	148	0·429	0·35	0·82
28	−60	27·7	5·35	0·486	0·379	0·948	0·150	335	140	0·418	0·34	0·81
25	−45	27·8	5·05	0·477	0·379	0·949	0·150	328	132	0·401	0·31	0·77
26	−45	27·5	5·02	0·509	0·378	0·956	0·150	348	130	0·373	0·34	0·91
32	−30	28·1	5·10	0·524	0·380	0·944	0·150	362	134	0·371	0·29	0·78
33	−30	27·8	5·11	0·510	0·379	0·949	0·150	351	133	0·379	0·28	0·74
2	0	28·5	4·55	0·538	0·382	0·935	0·150	375	121	0·323	0·30	0·93
3	0	25·3	5·31	0·541	0·368	1·000	0·149	355	128	0·361	0·29	0·80
5	0	24·9	5·03	0·556	0·366	1·010	0·149	362	120	0·331	0·31	0·94
9	30	28·0	6·57	0·516	0·380	0·945	0·150	355	172	0·486	0·34	0·70
10	30	27·4	6·38	0·541	0·377	0·957	0·150	369	164	0·445	0·34	0·76
17	30	27·8	6·74	0·548	0·379	0·949	0·150	377	176	0·467	0·36	0·77
11	45	28·2	7·45	0·518	0·381	0·941	0·150	359	197	0·547	0·42	0·77
12	45	28·4	7·05	0·508	0·382	0·938	0·150	353	187	0·531	0·40	0·75
13	60	29·1	8·81	0·526	0·385	0·924	0·151	370	239	0·645	0·46	0·71
14	60	29·2	8·57	0·533	0·386	0·922	0·151	376	233	0·620	0·47	0·76
15	75	31·0	12·97	0·549	0·394	0·890	0·151	399	371	0·931	0·52	0·56
16	75	30·9	11·89	0·477	0·393	0·891	0·151	346	340	0·982	0·52	0·53
31	75	31·2	11·85	0·561	0·395	0·887	0·152	409	341	0·834	0·60	0·72

TABLE 1. Summary of experimental conditions and results. (Average experimental conditions: $\phi_0 = 0{\cdot}0052$ cm^{-1}; $R_S = 362000$; $\kappa_T/\kappa_S = 83{\cdot}0$.)

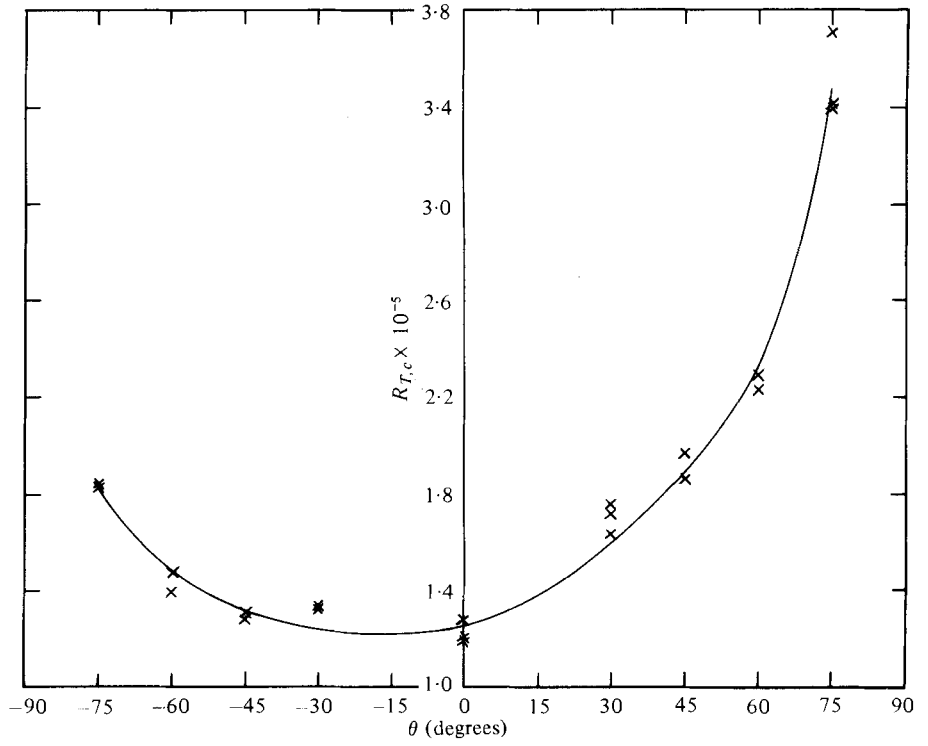

FIGURE 5. Experimental critical thermal Rayleigh number for all angles of inclination tested.

ratio of thermal diffusivity κ_T to solute diffusivity κ_S appropriate to the mean temperature is 83. Experimental values of R_T and R_S are computed using ΔT_c and initial density gradient ϕ_0 as determined in § 3.1. Values of fluid properties α, ν, and κ_T correspond to conditions at the centre of the slot. These conditions are 10 % salt concentration and the mean of the temperatures of the hot and cold boundaries at the time of the onset of instability. Thermal conductivity (k), density (ρ), and specific heat (c_p) required for the computation of κ_T ($= k/\rho c_p$) are evaluated using a least-squares second-degree polynomial fitted to the salt-properties data reported by Kaufmann (1960). A check on the properties ρ and α ($= -\rho^{-1} d\rho/dT$) is available using a polynomial developed by Ruddick & Shirtcliffe (1979). Viscosity of the salt solution is evaluated by a polynomial taken from *International Critical Tables* (1933).

The mean value of R_S calculated in this manner for all the experimental runs is 362000, with a standard deviation σ of 19000 and scattering of data confined to $\pm 2{\cdot}5\sigma$. Assuming an error of $\pm 0{\cdot}05$ % in fluid properties, ± 3 % in ϕ_0, $\pm 1{\cdot}5$ % in ΔT and 1 % in D, uncertainties in R_T and R_S are estimated to be about 5 %.

4.1. *Critical conditions*

The critical thermal Rayleigh number $R_{T,c}$ is shown as a function of inclination angle θ in figure 5. A smoothed curve is drawn through the data points. It is seen that the $R_{T,c}$ is non-symmetrical with respect to $\theta = 0°$; heating of the lower wall is more stable than heating of the upper wall at any given θ up to 75°. This is the result of the

basic flow field generated separately by the density stratification and by thermal convection.

When the lower wall is heated, $\theta > 0°$, the buoyancy layer and the thermal layer augment each other. The flow is upward along the lower wall and downward along the upper wall. This slow but constant transport of fluid generates a steady state in which the vertical salt gradient is larger than the initial value while the horizontal gradient of the overall density (due to salt and temperature) remains essentially zero. When the upper wall is heated, the flow in the thermal layer opposes that in the buoyancy layer. As a result the vertical salt gradient in the steady state is less than the initial value. Since the sideways double-diffusive instability observed in these experiments is the result of the destabilizing effects of the horizontal temperature gradients overcoming the stabilizing effects of the vertical salt gradient, it is then not surprising that the system is more stable with the lower wall heated than with the upper wall heated.

In all of the tests, no oscillatory instability was detected. This is further confirmed by stability analysis (Paliwal & Chen 1980).

The vertical dimension of the cells increases as inclination (θ) of the slot increases. Pictures of the instability of various inclinations taken after about 3–5 minutes of its first visual detection were used to make estimates of the average cell heights at different angles. Average cell size was obtained by measuring the total thickness of several layers in the z direction and then computing the average thickness ($\lambda \cos\theta$) of a cell in the vertical direction. This quantity is compared with the natural length scale

$$(h = \alpha \Delta T / \phi_0)$$

in figure 6. In general, the natural length scale h is larger than the cell size actually measured. The ratio of actual size to the natural length scale is approximately 0·88; at positive θ it ranges from 0·53 to 0·76 while at negative θ it ranges from 0·63 to 0·91. Chen *et al.* (1971) have reported a range from 0·67 to 0·97 for this ratio for their experiments in a wide tank and with impulsive heating of one of the side walls.

4.2. *Flow-visualization results*

Photographic records of the onset and evolution of instability during the first hour after its detection at various inclinations are presented in figures 7–15 (plates 1 to 9). The obstruction in the middle of the slot, seen in some of the photographs, is due to the presence of small sampling tubes. These were mounted to permit withdrawal of fluid samples to determine the solute concentration gradient across the slot for the purpose of verifying the basic flow model. A documentation of the many qualitative features of the secondary flow is as follows.

Many features of the flow following the onset of instability are common to all the runs irrespective of the angle of inclination. The occurrence of instability is in the form of approximately horizontal layers extending from the hot wall to the cold wall. Once they appear, the layered region gradually spreads, usually upward (cf. § 3.2), with the appearance of more and more layers adjacent to the previous ones. In about 10–15 min there may be seen a common tendency of each layer to grow in vertical size owing to continuous intensification of the motion inside it. At t = 15–30 min, the number of layers start decreasing owing to gradual merging of weakly convecting layers with strongly convecting layers. This process sometimes continues for several days until the final state of complete mixing of the fluid in the entire tank.

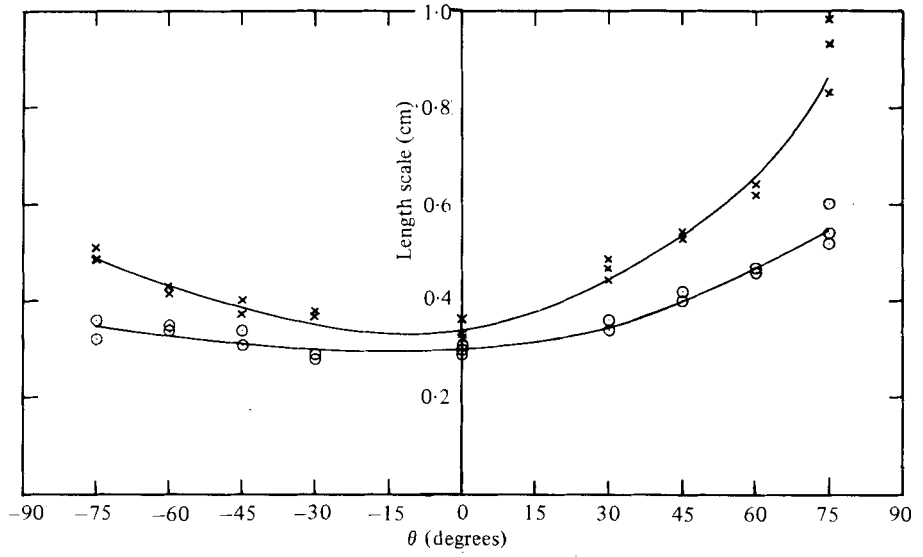

FIGURE 6. Experimental critical wavelength in the vertical direction, $\lambda \cos\theta$ (⊙), and the natural length scale h (×) for all angles of inclination tested.

Besides the common features of the secondary flow at different angles, some striking differences are readily seen. In the case of negative angles (heating from above), the motion within the layers is hardly discernible (figures 7–10). Positive angles (heating from below), in contrast, are associated with vigorous motion inside the layers, particularly at large θ. At $\theta = -75°$ (figure 7), the intensity of motion is so low that all the interfaces and layers are almost intact at the end of $t = 62$ min. Correspondingly, at $\theta = +75°$ (figure 15), breaking of the interfaces has begun as early as $t = 11$ min or perhaps even earlier. By $t = 15$ min, the interface has been completely destroyed. At later times, the vigorous motion inside the layer and the rapid expansion rate of the mixed region can be clearly seen.

Comparison of pictures at positive angles 0°–75° (figures 11–15) show that, as θ increases, the cell erosion process becomes faster and faster, owing to more and more intensified motion inside the cells. At $\theta = 0°$, there is no turbulent motion visible inside the cells at any time. At least one of the oldest cells has grown about 4–5 times its original size at $t = 63$ min. A large number of cells, although bigger than their original size, are still present. Compared to $\theta = 0°$, there is considerably more mixing within the cells for $\theta = 30°$. This trend continues for $\theta = 45°$, 60° and 75°. At the end of approximately 1 h, breaking of the interfaces between layers for these angles may be seen to have taken place at an increasingly faster rate.

An extremely beautiful photographic record of a row of vortices in the case of $\theta = 75°$ is shown in figure 15. At $t = 10$ min, there are two fairly well-defined layers with no apparent danger to their survival. Suddenly at $t = 11$ min, a blob of fluid in the bottom of the lower layer is seen rising vertically and breaking straight into the interface above, quite forcefully. The result as seen on the shadowgraph is a vortex with its axis almost coinciding with the plane of the interface. More vortices, perhaps induced by the first one, immediately follow. At $t = 13$ and 14 min, there are four vortices in a row, surprisingly pentagonal in cross-section. The sense of the vortex motion (clockwise) is

opposite to the shear across the interface. The creation of vortices tends to reverse the flow direction in the vicinity of the interface, and in addition introduces large amounts of localized circulation in the fluid. A very effective break-up of the interface takes place, followed by vigorous mixing of the fluid of the two originally separate layers. It is strange that break-up of the interface takes place in such a peculiar way at $\theta = 75°$. Actually, the sudden vertical rise of the blobs of fluid may also be seen for $\theta = 45°$ (figure 13) in several layers at $t = 9$ min, and for $\theta = 60°$ (figure 14) at $t = 11$ min. In these cases, however, the rise of the blob is not sufficiently intense to break the upper interface. A possible explanation of the peculiarity of the $\theta = 75°$ case may lie in the effect of the presence of a relatively large vertical destabilizing component of the temperature gradient ($R_T \sin\theta$). As soon as the first instability sets in, the original motion within a layer is toward the hot wall near the bottom and away from the hot wall near the top. The net tendency of this flow is to reduce the solute density gradient within the layer. The continuously decreasing gradient eventually becomes unstable owing to the heating-from-below effect of the vertical component of the imposed temperature gradient, possibly for all positive angles. At $\theta = 75°$, the effect of this component is probably too large to be contained within a single layer.

The financial support of the National Science Foundation through Grant ENG 73-03545-A01 is gratefully acknowledged.

REFERENCES

CHEN, C. F. 1975 Double-diffusive convection in an inclined slot. *J. Fluid Mech.* **72**, 721–729.

CHEN, C. F. 1978 Double-diffusive instability in a density-stratified fluid along a heated inclined wall. *J. Heat Transfer* **100**, 653–658.

CHEN, C. F., BRIGGS, D. G. & WIRTZ, R. A. 1971 Stability of thermal convection in a salinity gradient due to lateral heating. *Int. J. Heat Mass Transfer* **14**, 57–65.

CHEN, C. F., PALIWAL, R. C. & WONG, S. B. 1976 Cellular convection in a density stratified fluid: Effect of inclination of the heated wall. *Proc.* 1976 *Heat Transfer & Fluid Mech. Inst.*, pp. 18–32. Stanford University Press.

CHEN, C. F. & SANDFORD, R. D. 1976 Size and shapes of salt fingers near marginal state. *J. Fluid Mech.* **78**, 601–607.

CHEN, C. F. & SANDFORD, R. D. 1977 Stability of time-dependent double-diffusive convection in an inclined slot. *J. Fluid Mech.* **83**, 83–95.

CHEN, C. F. & SKOK, M. W. 1974 Cellular convection in a salinity gradient along a heated inclined wall. *Int. J. Heat Mass Transfer* **17**, 51–60.

WEAST, R. C. 1977–1978 *Handbook of Chemistry and Physics*, 58th edn, pp. D224–225. Cleveland, Ohio: C.R.C.

HART, J. E. 1971 On sideways diffusive instability. *J. Fluid Mech.* **49**, 279–288.

International Critical Tables of Numerical Data (1933), vol. II, p. 328. National Research Council; McGraw-Hill.

KAUFMAN, D. W. 1960 *Sodium Chloride*. New York: Reinhold.

LINDEN, P. F. & WEBER, J. E. 1977 The formation of layers in a double-diffusive system with a sloping boundary. *J. Fluid Mech.* **81**, 757–773.

PALIWAL, R. C. 1979 Double-diffusive convective instability in an inclined fluid layer. Ph.D. thesis, Department of Mechanical, Industrial and Aerospace Engineering, Rutgers University.

PALIWAL, R. C. & CHEN, C. F. 1980 Double-diffusive instability in an inclined fluid layer. Part 2. Stability analysis. *J. Fluid Mech.* **98**, 769–785.

PHILLIPS, O.M. 1970 On flows induced by diffusion in a stably stratified fluid. *Deep-Sea Res.* **17**, 435–443.

RUDDICK, B. R. & SHIRTCLIFFE, T. G. L. 1979 Data for double diffusers (physical properties of aqueous salt–sugar solutions). *Deep-Sea Res.* **26**, 775–787.

SHIRTCLIFFE, T. G. L. 1969 An experimental investigation of thermosolutal convection at marginal stability. *J. Fluid Mech.* **35**, 677–688.

THORPE, S. A., HUTT, P. K. & SOULSBY, R. 1969 The effect of horizontal gradients on thermohaline convection. *J. Fluid Mech.* **38**, 375–400.

TURNER, J. S. & CHEN, C. F. 1974 Two-dimensional effects in double-diffusive convection. *J. Fluid Mech.* **63**, 577–592.

VERONIS, G. 1965 On finite amplitude instability in thermohaline convection. *J. Mar. Res.* **23**, 1–17.

WRIGHT, J. H. & LOEHRKE, R. I. 1976 The onset of thermohaline convection in a linearly stratified horizontal layer. *J. Heat Transfer* **98**, 558–563.

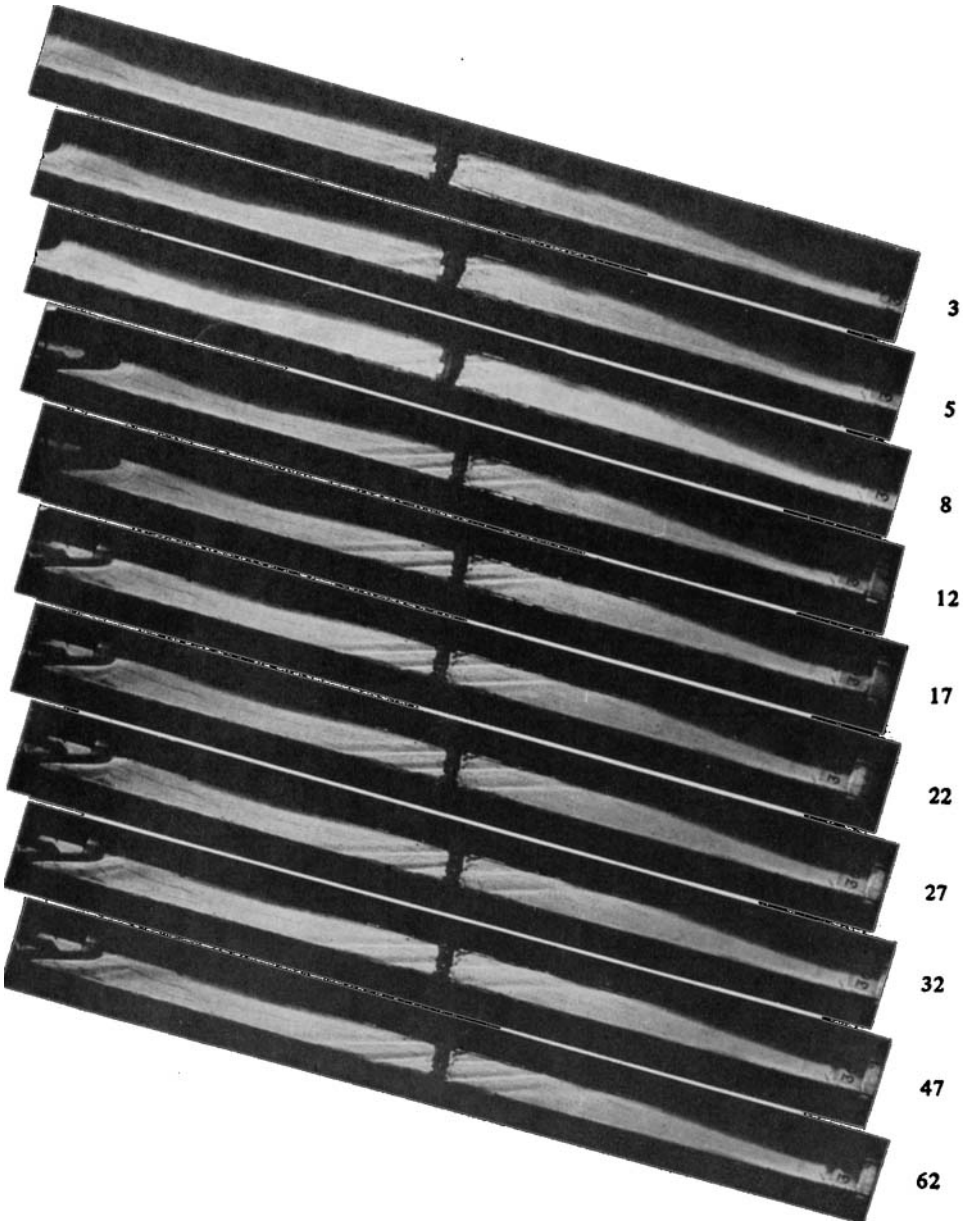

FIGURE 7. Onset and evolution of instability at $\theta = -75°$. The numbers denote time in minutes after the instability is first detected.

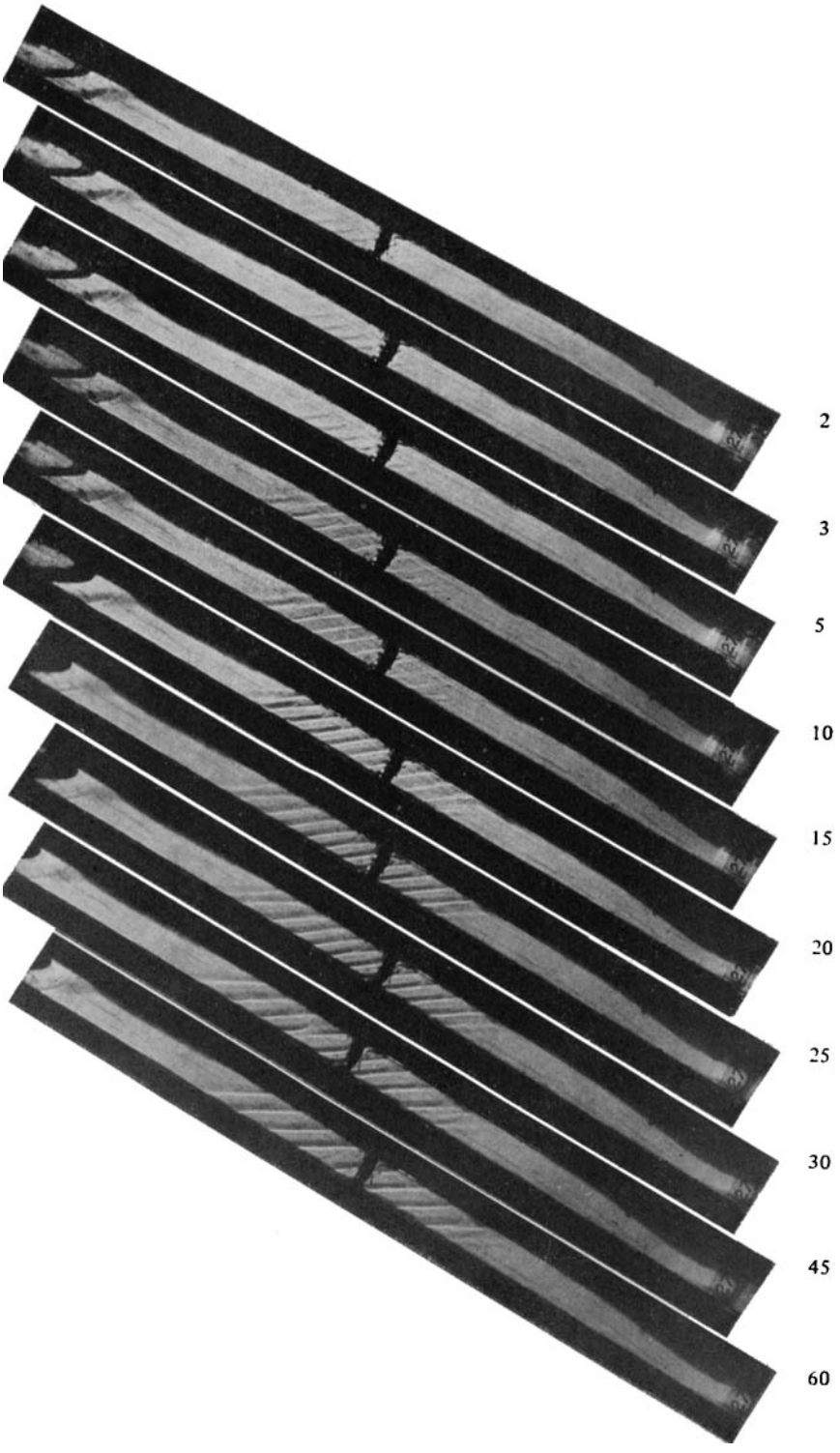

FIGURE 8. Onset and evolution of instability at $\theta = -60°$. The numbers denote time in minutes after the instability is first detected.

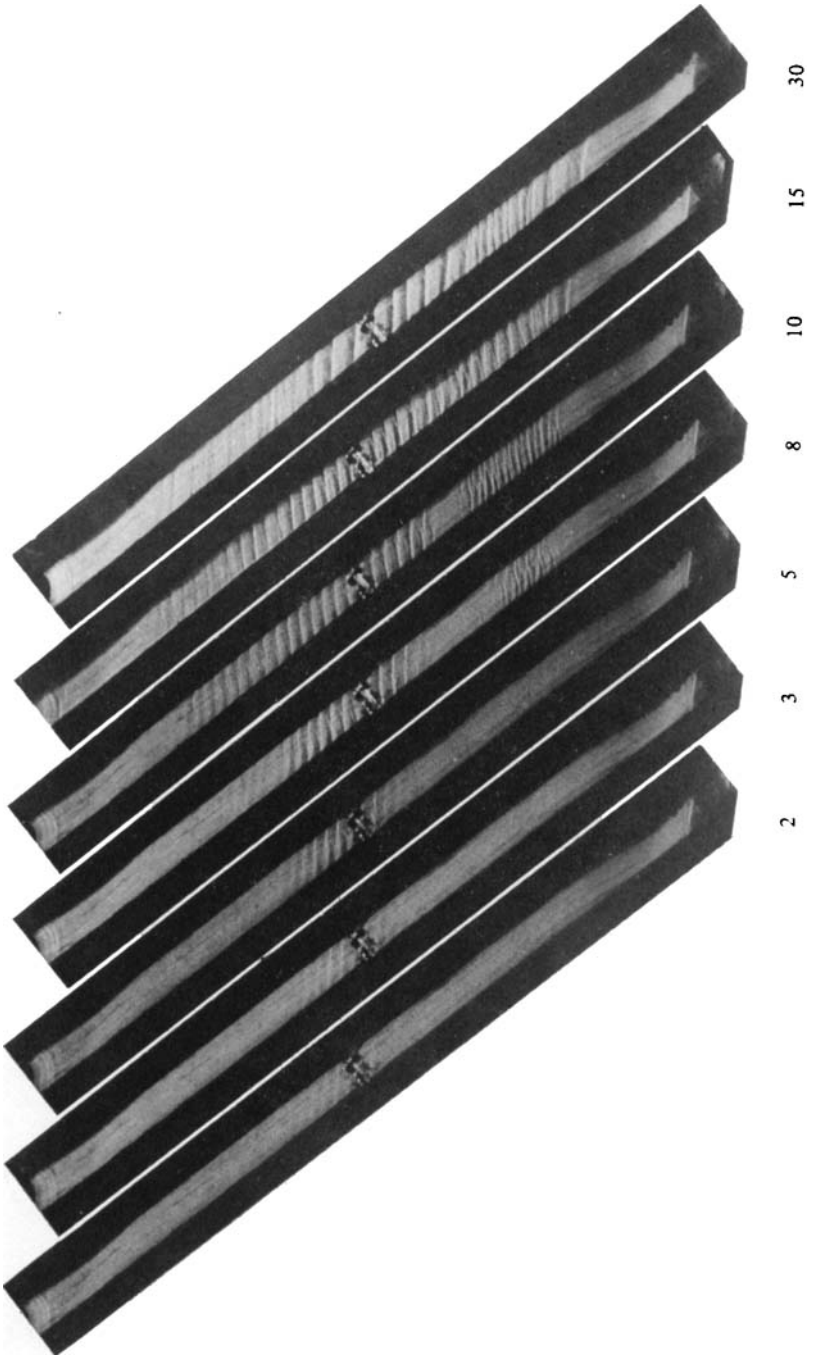

FIGURE 9. Onset and evolution of instability at $\theta = -45°$. The numbers denote time in minutes after the instability is first detected.

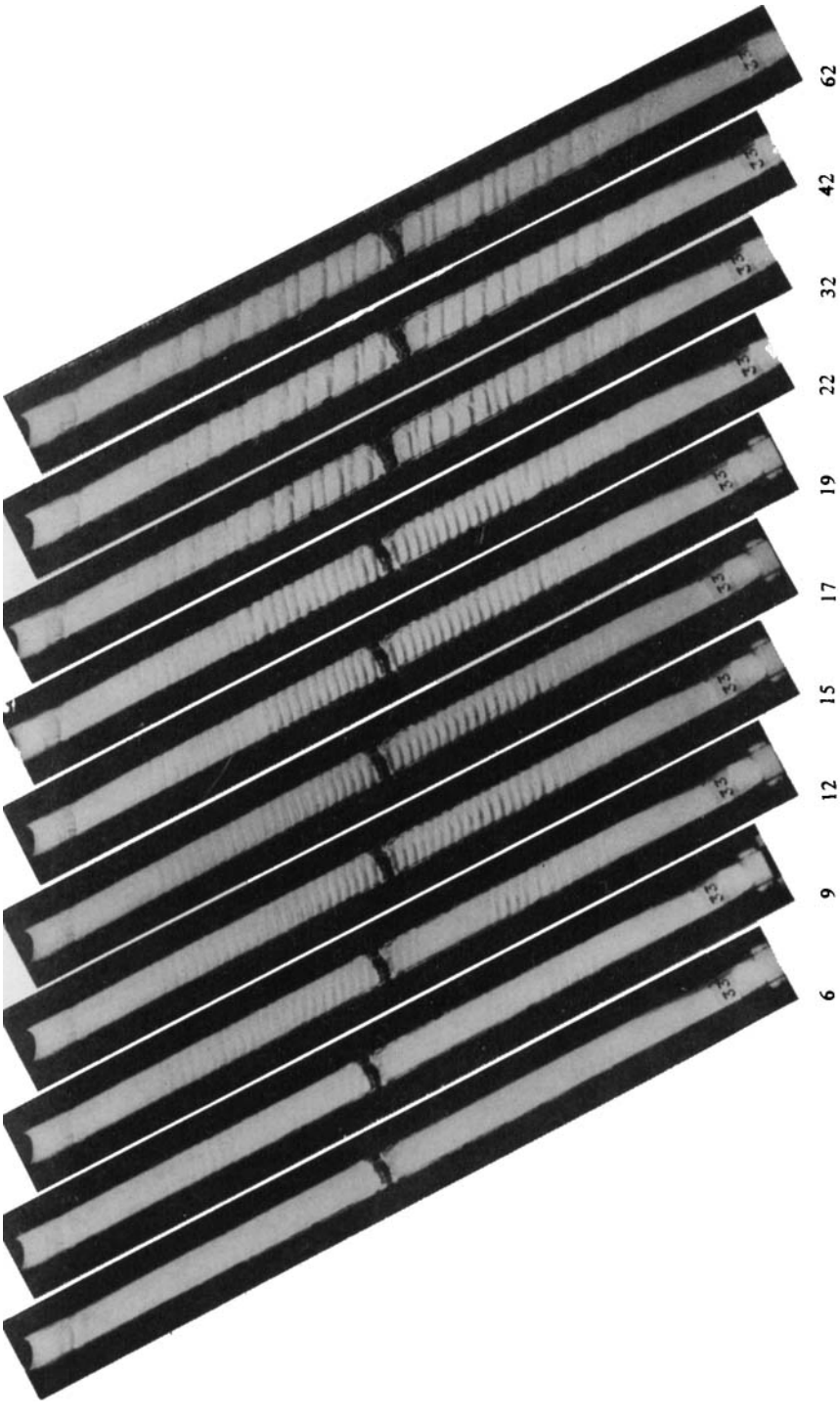

FIGURE 10. Onset and evolution of instability at $\theta = -30°$. The numbers denote time in minutes after the instability is first detected.

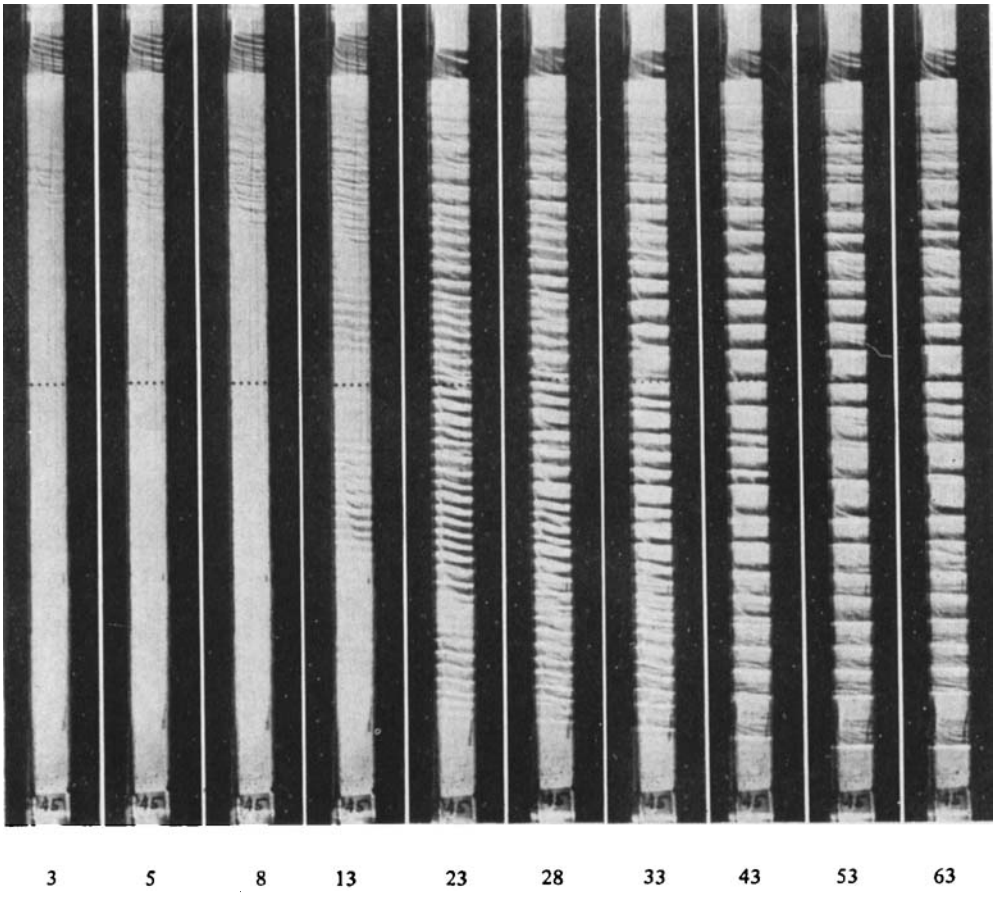

FIGURE 11. Onset and evolution of instability at $\theta = 0°$. The numbers denote time in minutes after the instability is detected.

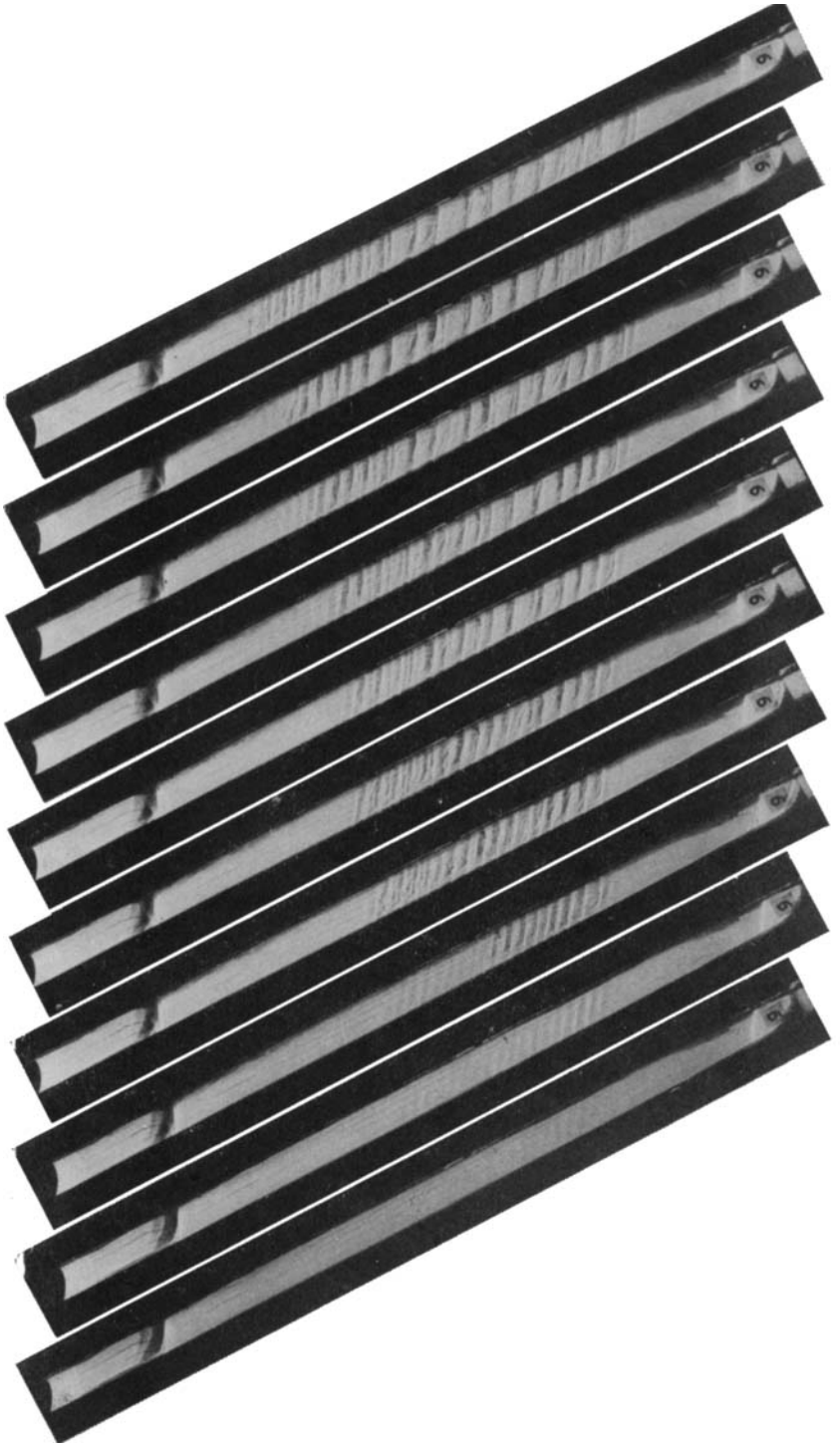

FIGURE 12. Onset and evolution of instability at $\theta = +30°$. The numbers denote time in minutes after the instability is detected.

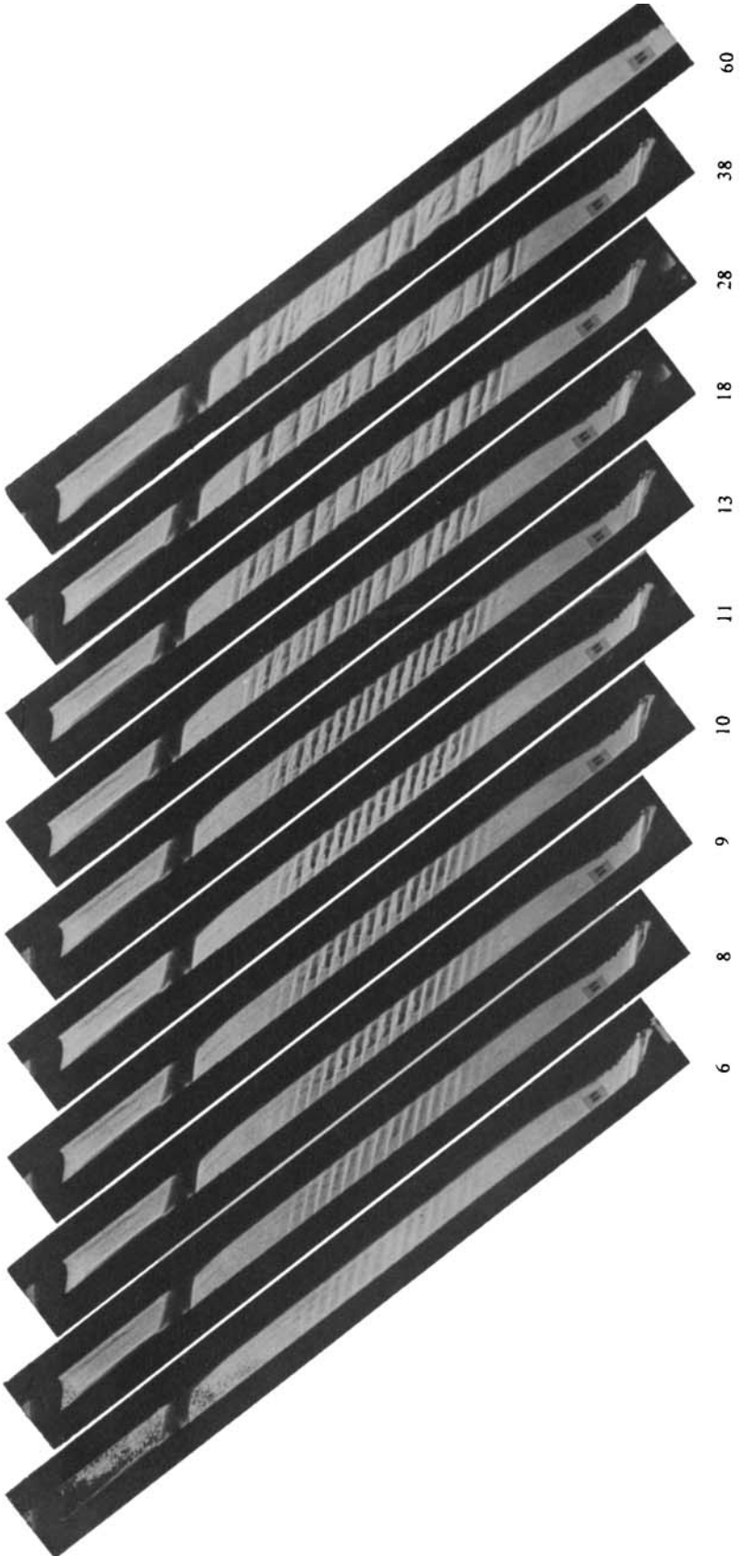

FIGURE 13. Onset and evolution of instability at $\theta = +45°$. The numbers denote time in minutes after the instability is detected.

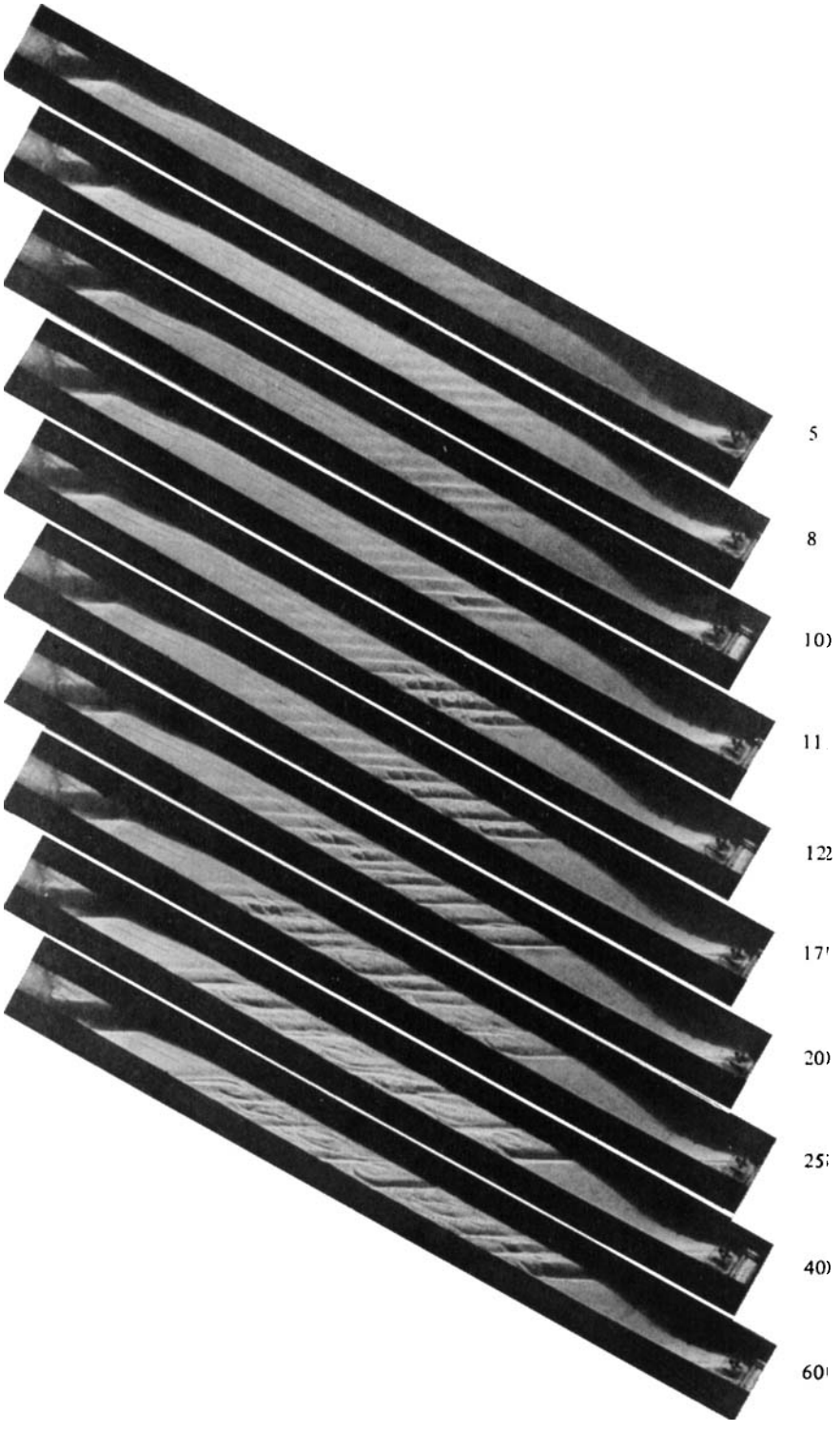

FIGURE 14. Onset and evolution of instability at $\theta = +60°$. The numbers denote time in minutes after the instability is detected.

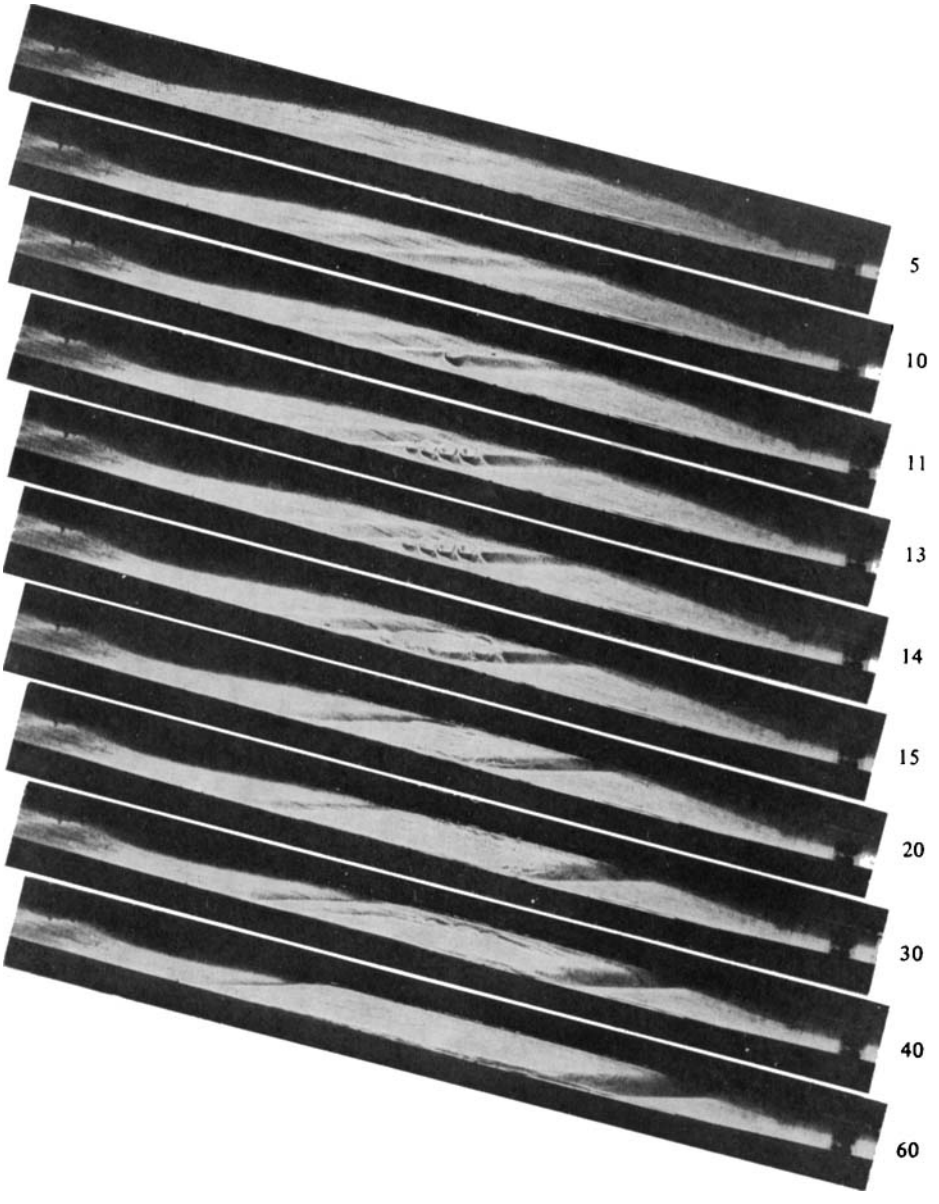

FIGURE 15. Onset and evolution of instability at $\theta = +75°$. The numbers denote time in minutes after the instability is detected.